Organic Semiconductors

DOI: 10.1002/ange.201210085

Tetraazabenzodifluoranthene Diimides: Building Blocks for Solution-Processable n-Type Organic Semiconductors**

*Haiyan Li, Felix Sunjoo Kim, Guoqiang Ren, Emily C. Hollenbeck, Selvam Subramaniyan, and Samson A. Jenekhe**

Organic electronics, which exploits organic molecular materials as semiconductors and active elements in devices, is a rapidly growing interdisciplinary field of research. Its applications include organic field-effect transistors (OFETs), logic circuits, memories, organic light-emitting diodes and displays, lighting, and organic photovoltaic devices (OPVs).[1] Both hole-conducting (p-type) and electron-conducting (n-type) organic semiconductors are required in these device applications. In the past two decades, considerable progress has been made in developing p-type organic semiconductors of diverse molecular structures, which have enabled advances in device performance and understanding of charge transport.[1a,d,f] In contrast, n-type organic semiconductors have limited molecular diversity, their device performance (e.g. electron mobility) is still lower than that of p-type organic materials, and the understanding of electron transport is not as good as that of p-type materials.[1c,2]

Current n-type organic semiconductors are roughly of two types: 1) those obtained by functionalizing known p-type molecules (e.g. oligothiophenes) with electron-withdrawing groups;[3] and 2) those constructed from distinct electron-deficient polycyclic rings as exemplified by naphthalene diimide (NDI) and perylene diimide (PDI).[4] Functionalization with electron-withdrawing groups can efficiently increase the electron affinity. However, the substituents may reduce the planarity of the parent molecules because of steric effects; the distortion from planarity leads to interruption of the π-electron orbital overlap and can adversely affect charge transport.[5] Among current n-type organic semiconductors, naphthalene diimides (NDIs) and perylene diimides (PDIs) and their derivatives have shown promising electron-transport properties.[4,6]

We report herein the first examples of heterocyclic diimides, tetraazabenzodifluoranthene diimides (BFIs); the synthesis involves fusion of a synthetically tunable tetraazaanthracene core and two naphthalene imide units (Scheme 1). This molecular design aims to: 1) obtain high electron affinity by combining the electron-deficient imine nitrogen containing aromatic groups with the dicarboxylic acid imide functionality; 2) form a large rigid ladder-type structure: in comparison to NDI and PDI, the 11-ring BFI system has an even larger framework, which can further extend the π conjugation, promote intermolecular orbital overlap, and improve carrier mobilities; 3) potentially tune the optical and electronic properties through nitrogen protonation or quaternization;[7] and 4) enable fine-tuning of the electronic structure, solution processability, and solid-state morphology. Further molecular modification of the BFIs can either occur at the imide nitrogen atoms, the "bay" area, or even the "core" itself. Unlike the sterically crowded NDI and PDI rings, the new tetraazabenzodifluoranthene diimide has two

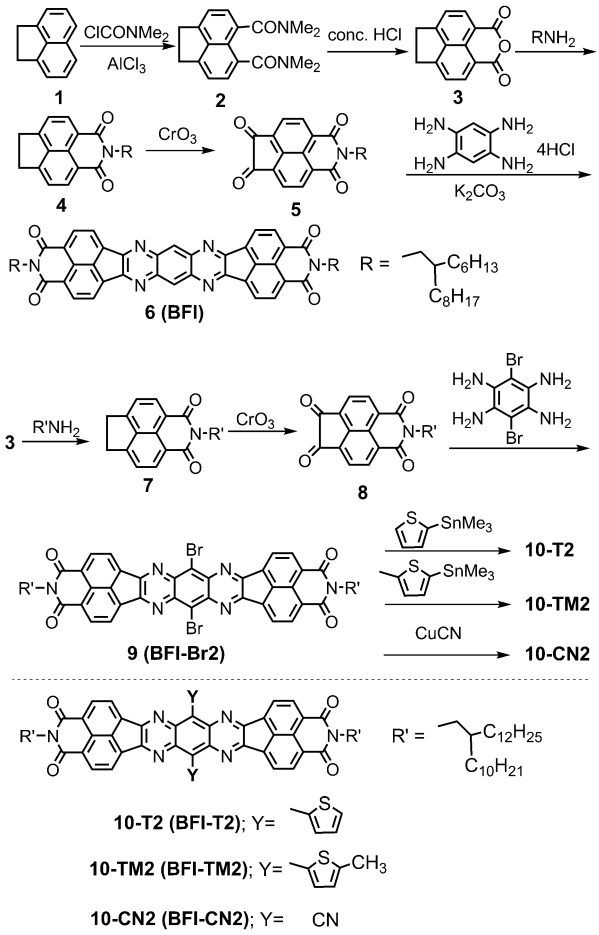

Scheme 1. Synthesis of BFIs.

[*] Dr. H. Li, Dr. F. S. Kim, G. Ren, E. C. Hollenbeck, Dr. S. Subramaniyan, Prof. Dr. S. A. Jenekhe
Department of Chemical Engineering and Department of Chemistry
University of Washington
Seattle, WA 98195-1750 (USA)
E-mail: jenekhe@u.washington.edu

[**] We thank Dr. Werner Kaminsky for obtaining the X-ray single crystal structure of BFI. This work was supported by the NSF (DMR-1035196), Office of Naval Research (ONR) (N00014-11-1-0317), and Solvay S. A.

Supporting information for this article is available on the WWW under http://dx.doi.org/10.1002/anie.201210085.

symmetric and easily accessible sites for substitution. We envision that the new dibromide derivative BFI-Br2 will become an important intermediate for the design and synthesis of new organic/polymer semiconductors.

Scheme 1 presents the synthesis of BFI and its derivatives. Starting from acenaphthene (**1**), the diketo intermediates 2-(2-hexyldecyl)-1*H*-indeno[6,7,1-def]isoquinoline-1,3,6,7(2*H*)-tetraone and 2-(2-decyltetradecyl)-1*H*-indeno[6,7,1-def]isoquinoline-1,3,6,7(2*H*)-tetraone (**5** and **8**) were synthesized in four steps. 1,2-Diketone is well-known to readily react with *ortho*-arylenediamine to form a pyrazine ring.[8] By taking advantage of this reaction, BFI (**6**) and BFI-Br2 (**9**) were synthesized in the reactions of **5** with 1,2,4,5-benzenetetraamine tetrahydrochloride and **8** with 3,6-dibromobenzene-1,2,4,5-tetraamine, respectively. The reaction of the key precursor BFI-Br2 with 2-tributylstannylthiophene or 5-methyl-2-trimethylstannylthiophene under standard Stille cross-coupling reaction conditions afforded BFI-T2 (compound **10**-T2) and BFI-TM2 (compound **10**-TM2), respectively. The dicyano derivative BFI-CN2 (**10**-CN2) was prepared by the reaction of BFI-Br2 with CuCN in DMF. BFI-T2 and BFI-TM2 were isolated as green solids, and BFI-CN2 was isolated as a yellow solid. The parent BFI has a poor solubility in aprotic organic solvents, but can be dissolved in organic acids (e.g. trifluoroacetic acid) or organic solvent/organic acid solvent mixtures. With two bromo groups, BFI-Br2 has moderate solubility and can be dissolved in warm organic solvents. Fortunately, attachment of substituent groups dramatically enhances the solubility of the BFI derivatives. BFI-CN2, BFI-T2, and BFI-TM2 all have good solubility in organic solvents (chloroform, dichloromethane, toluene, etc.).

Thermogravimetric analysis showed that all the molecules are thermally stable with high thermal decomposition temperatures ($T_d \geq 400\,^{\circ}C$; Figure S6 and Table S2 in the Supporting Information). Differential scanning calorimetry (DSC) showed that the parent BFI (**6**) has no detectable phase transitions in the temperature range from 30 °C to 250 °C, whereas BFI-T2, BFI-TM2, and BFI-CN2 each exhibited multiple melting and liquid-crystalline transitions (Figure S7 and Table S2 in the Supporting Information). The high thermal stability of BFI arises from the dense packing of the large planar backbones and strong intermolecular interactions induced by the polar imide groups and the imine nitrogen atoms. On the other hand, the substituents on BFI-CN2, BFI-T2, and BFI-TM2 increase the free space between the molecular backbones and enable the observed thermal transitions.

Single-crystal X-ray diffraction analysis of BFI (Figure 1) showed that the BFI molecules are aligned in a triclinic unit cell with $a = 4.681(4)$ Å, $b = 16.30(2)$ Å, $c = 17.554(16)$ Å, $\alpha = 94.08(5)°$, $\beta = 93.92(3)°$, $\gamma = 95.36(6)°$.[9] The polycyclic BFI ring has a planar geometry involving both the diimide groups and tetraazabenzodifluoranthene backbone (Figure 1 a). The molecules of BFI form a slipped face-to-face π–π stacking, and the displacement between two neighboring molecules is less than one sixth of the length of the molecule; this ratio is relatively smaller than that of the NDI and PDI molecules,[4d,i] which might be due to the much longer length of BFI and stronger intermolecular interactions induced by the imine

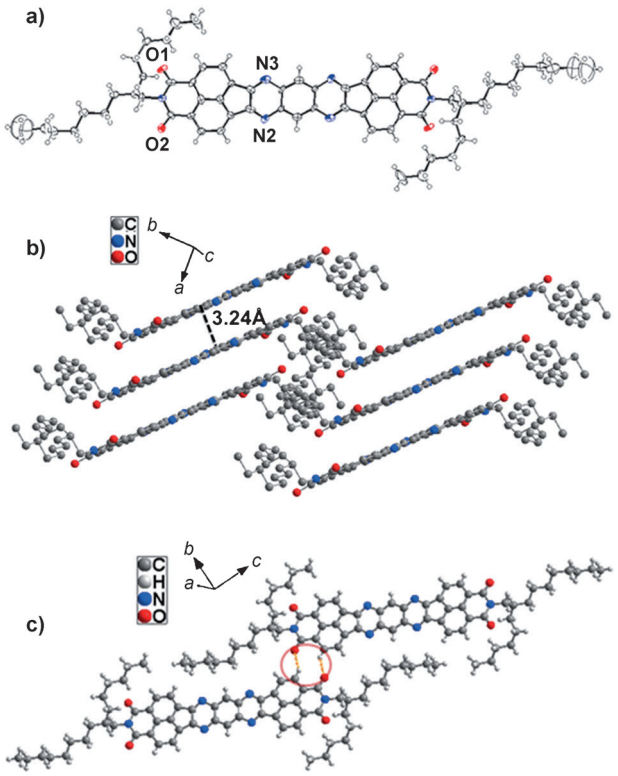

Figure 1. Crystal structure of BFI. a) Thermal ellipsoid plot with ellipsoids drawn at 50% probability level. b) Face-to-face π–π stacking with an interplanar distance of 3.24 Å. c) C–H···O hydrogen bonding between stacks (dashed lines in red circle).

nitrogen atoms. The neighboring BFI molecules feature a short vertical distance of 3.24 Å, which is significantly shorter than the interplanar distance of graphite (3.35 Å)[10] and suggests strong π–π interactions (Figure 1 b). Furthermore, we found that π–π stacking is not the only driving force that controls the assembly of BFI molecules. Figure 1 c shows another type of close contacts, C–H···O hydrogen bonds, which are shorter than the sum of van der Waals radii and exist between the neighboring stacks. In these hydrogen bonds, the oxygen atom on the carbonyl group and the *ortho*-carbon atom on the naphthalene ring of the neighboring molecule function as the hydrogen acceptor and donor, respectively. The H···O distance is measured to be 2.44 Å and the C-H···O angle to be 140.1°. Both the rigid planar structure and strong intermolecular interactions are highly desirable for achieving high crystallinity, high degree of molecular orbital coupling, and efficient carrier transport.

X-ray quality single crystals of BFI-T2, BFI-TM2, or BFI-CN2 could not be obtained under normal solution conditions. X-ray diffraction (XRD) from solution-cast films was thus used to evaluate the crystallinity of this series of molecules. The intense first Bragg reflection and its higher-order reflections from BFI films were observed at 3.0°, 9.3°, 12.3°, 18.5°, and 21.2° corresponding to a d-spacing of 2.9 nm, which is close to the length of the long axis of the BFI molecules and thus is assigned to the edge-to-edge packing of the BFI molecules along the long axis (Figure S8 in the Supporting Information). BFI-T2 and BFI-TM2 exhibit similar X-ray

diffraction patterns as BFI, although the reflection angles are slightly different: the long-axis reflections of BFI-T2 and BFI-TM2 are observed at 2.9° ($d = 3.1$ nm) and 3.2° ($d = 2.8$ nm), respectively. The 2-thienyl and 5-methyl-2-thienyl groups significantly enlarge the d-spacing of the short-axis reflections, which are observed at 7.5° ($d = 11.8$ Å) for BFI-T2 and 7.4° ($d = 11.9$ Å) for BFI-TM2 in comparison to that of BFI at 10.5° ($d = 8.5$ Å). Unlike BFI, BFI-T2, and BFI-TM2 films, which favor edge-to-edge packing, BFI-CN2 is less crystalline with two broad peaks at 25.7°(d=3.55 Å) and 20.0° (d = 4.50 Å), corresponding to the face-to-face π–π stacking. Such a substituent-dependent solid-state morphology can be expected to affect the charge transport properties of these materials in devices.

Effects of the substituent group on the electronic structure of BFI molecules were examined by UV/Vis absorption spectroscopy of BFIs in dilute solution and as thin films. The absorption maxima, molar absorptivity (ε_{max}), absorption coefficient (α_{max}), and optical absorption edge band gaps are collected in Table S2 in the Supporting Information. In solution (Figure 2a), all the BFIs show a common high-energy absorption band centered at around 400 nm with ε_{max} of $(1.0–1.7)\times10^5\,\text{M}^{-1}\text{cm}^{-1}$, which is thus assigned to the transition characteristic of the tetraazabenzodifluoranthene diimide chromophore. A new low-energy band appears in the region of 460–700 nm ($\varepsilon_{max} = (1.3–1.8)\times10^4\,\text{M}^{-1}\text{cm}^{-1}$) for both BFI-T2 and BFI-TM2, which is consistent with the facts that BFI and BFI-CN2 are yellow, whereas BFI-T2 and BFI-TM2 are green in color. The observed low-energy absorption band in BFI-T2 and BFI-TM2, which is absent in BFI and BFI-CN2, originates from intramolecular charge transfer between the electron-deficient BFI and electron-donating thiophene or methylthiophene substituents.[11] Going from dilute solution to thin films (Figure S9 in the Supporting Information), the high-energy absorption band is blue-shifted by 20–40 nm suggesting an H aggregation in the solid state. In contrast, the lower-energy absorption of BFI-T2 and BFI-TM2 becomes significantly red shifted (ca. 100 nm), which could be understood as a result of enhanced intramolecular charge transfer enabled by the strong intermolecular interactions.[11] BFI and BFI-CN2 have energy gaps of 2.43–2.50 eV, whereas BFI-T2 and BFI-TM2 have a significantly narrower band gap of 1.6 eV. We note that the band gap of BFI-T2 and BFI-TM2 is about 0.46 eV narrower than that of the NDI analogue (NDI-1TH),[4d] thus suggesting a higher degree of electron delocalization. The absorption coefficient (α_{max}) at the higher-energy absorption maximum of the thin films varied from $6.7\times10^4\,\text{cm}^{-1}$ in BFI-T2 to $1.4\times10^5\,\text{cm}^{-1}$ in BFI-CN2, which is indicative of strongly absorbing chromophores.

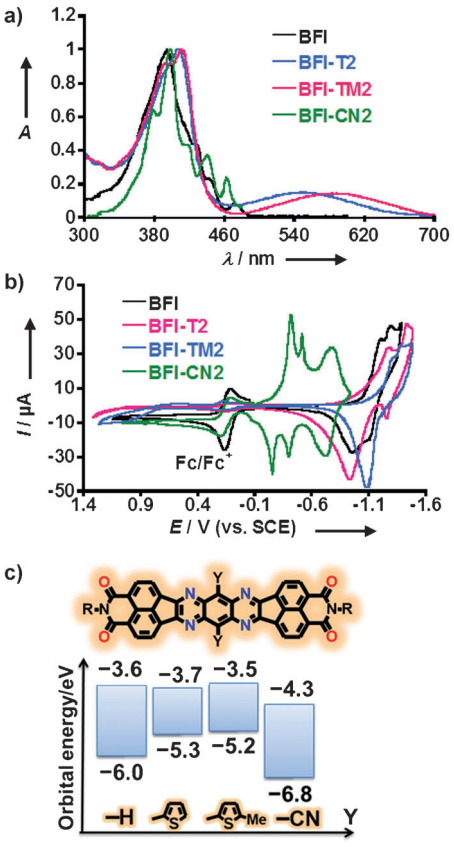

Figure 2. a) UV/Vis absorption spectra of BFIs in dilute solution (1.4–3.4 μM). b) Cyclic voltammograms of BFI molecules with the ferrocene/ferrocenium (Fc/Fc^+) couple as the internal reference. SCE = saturated calomel electrode. c) HOMO/LUMO energy levels of BFI molecules.

Figure 2b shows the thin-film cyclic voltammograms of the BFI molecules in acetonitrile with tetrabutylammonium hexafluorophosphate as the electrolyte (0.1M). BFI shows two quasi-reversible reduction waves at $E_{1/2} = -0.80$ V/−1.20 V, whereas the reduction peaks of BFI-T2 and BFI-TM2 are seen at more negative potentials of $E_{1/2} = -1.10$ V/−1.35 V and −1.23 V (peak), respectively. As expected, BFI-CN2, with two strong electron-withdrawing cyano groups attached, is reduced at much higher potentials with three reversible waves at $E_{1/2} = -0.34$ V/−0.46 V/−0.75 V. Accordingly, the resulting estimate of the lowest unoccupied molecular orbital (LUMO) energy level of BFI-CN2 is −4.32 eV, which is about 0.6–0.8 eV lower than that of BFI, BFI-T2, and BFI-TM2 and 0.4–0.6 eV lower than that of NDI and PDI.[4f] CV scans showed that BFIs either had a very weak oxidation or did not show any oxidation up to 1.2 V, indicative of a rather deep lying highest occupied molecular orbital (HOMO) energy level.

OFETs with bottom-gate geometry were fabricated by solution deposition of thin films to investigate the polarity and field-effect mobility of charge carriers in the BFIs. All the BFIs were found to exhibit n-channel charge transport characteristics in OFETs, thereby giving moderate to high electron mobilities (μ_e) of 0.021 to $0.12\,\text{cm}^2\text{V}^{-1}\text{s}^{-1}$ in the saturation region and excellent on/off current modulation (10^5–10^6; Figure 3 and Figures S10 and S11 in the Supporting Information). Among them, BFI-T2 thin films had the highest carrier mobility of $\mu_e = 0.12\,\text{cm}^2\text{V}^{-1}\text{s}^{-1}$ (Figure 3 and Figure S12 in the Supporting Information). The average field-effect electron mobilities of the parent BFI and BFI-TM2 were $0.03\,\text{cm}^2\text{V}^{-1}\text{s}^{-1}$ and $0.05\,\text{cm}^2\text{V}^{-1}\text{s}^{-1}$, respectively. Although BFI-CN2 has a higher electron affinity, it has the lowest electron mobility of $0.021\,\text{cm}^2\text{V}^{-1}\text{s}^{-1}$ in the transistors, which can be attributed to its poorer solid state packing as revealed by previously discussed XRD analysis. The BFIs

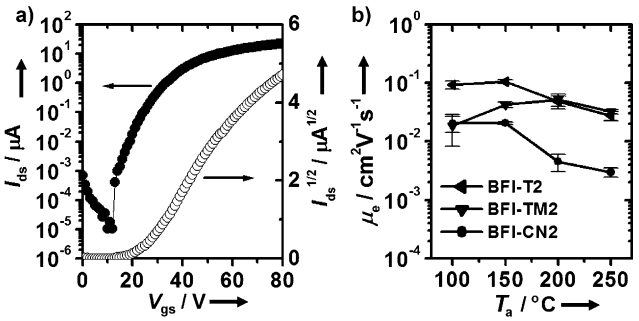

Figure 3. Transfer curve of a) BFI-T2 transistors after annealing at 150 °C (V_{ds} = 80 V). b) Electron mobilities of the BFIs measured in nitrogen as a function of annealing temperatures. I_{ds} = drain current, V_{gs} = gate voltage, V_{ds} = drain voltage.

showed an annealing temperature dependence of the electron mobility (Figure 3b). Annealing at 150 °C gave the highest mobility in accord with expectation from the DSC results. We note that the electron mobility derived from the linear region was generally 2–7-fold lower than the saturation mobility (Table S3 in the Supporting Information). Moderate threshold voltage (17–32 V) and hysteresis in forward and backward scans were also observed from the transistors (Figure S11 in the Supporting Information), possibly owing to traps at interfaces. The threshold voltage and the hysteresis, as well as the electron mobility could be significantly improved by interfacial engineering and optimization of device fabrication.[1]

In a preliminary evaluation of the potential of the BFIs to function as an electron acceptor in bulk heterojunction (BHJ) solar cells, we fabricated and tested devices of the type ITO/PEDOT:PSS/PSEHTT:BFI-T2(1:4 wt/wt)/LiF/Al under AM 1.5 solar illumination at 1 sun (100 mW cm^{-2}) in ambient air [ITO = indium tin oxide, PEDOT = poly(3,4-ethylenedioxythiophene), PSS = poly(styrenesulfonate)]. The donor polymer PSEHTT is a reported ethylhexyl derivative of thiazolothiazole copolymer.[12] The current density (J)–voltage (V) curves for these devices are shown in Figure 4a. The resulting photovoltaic parameters include an open circuit voltage (V_{oc}) of 0.79 V, a short-circuit current density (J_{sc}) of 5.14 mA cm^{-2}, and a fill factor (FF) of 0.44. A maximum power conversion efficiency of 1.80 % (average of 1.74 ± 0.06 %) was achieved. The EQE spectrum of the PSEHTT:BFI-T2 devices (Figure 4b) shows that the photoresponse begins near 800 nm, an important demonstration that the new electron acceptor can harvest photons from the near-IR region of the solar spectrum. The EQE spectrum has peaks of 31 % at 370 nm and 28 % at 630 nm. The J_{sc} value calculated by integrating the EQE spectrum is 4.85 mA cm^{-2}, which is within 6.0 % of the directly measured value. These preliminary results demonstrate that the BFIs are promising small-molecule, nonfullerene, acceptor materials for organic photovoltaics.

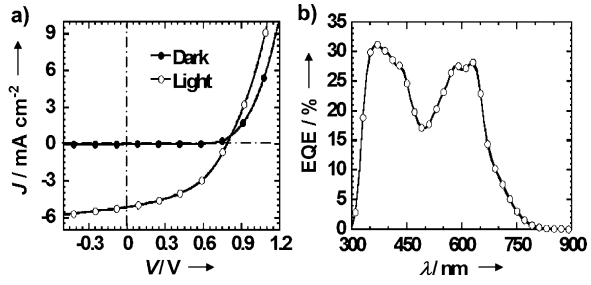

Figure 4. a) J–V characteristics of a PSEHTT:BFI-T2 (1:4 wt/wt) blend solar cell and b) the corresponding external quantum efficiency (EQE) spectrum.

In conclusion, we have successfully created new heterocyclic diimides as building blocks for developing n-type organic semiconductors. The X-ray single-crystal structure shows that tetraazabenzodifluoranthene diimide has a ladder-type planar conformation, which facilitates desirable solid-state molecular packing. The symmetric substitution sites on the core BFI framework provide a means for fine-tuning the electronic structure, solid-state morphology, and properties of the new class of n-type organic semiconductors. The BFIs combine large electron affinities (3.6–4.3 eV) with attractive optical band gaps of 2.5–1.6 eV by varying the substituents at the core position. Preliminary n-channel OFETs and BHJ solar cells based on solution-processed thin films gave an electron mobility of 0.12 cm^2 V^{-1} s^{-1} and a power conversion efficiency of 1.8 %, respectively, and thus demonstrated that the BFIs are promising n-type materials for organic electronics and nonfullerene photovoltaics. Indeed, BFI-T2 is the first nonfullerene small molecule that combines both high electron mobility in solution-processed n-channel OFETs and high power conversion efficiency as an electron acceptor in BHJ solar cells.

Received: December 18, 2012
Revised: March 17, 2013
Published online: April 15, 2013

Keywords: electron transport · energy conversion · field-effect transistors · semiconductors · solar cells

[1] a) C. Wang, H. Dong, W. Hu, Y. Liu, D. Zhu, *Chem. Rev.* **2012**, *112*, 2208; b) A. Mishra, P. Bäuerle, *Angew. Chem.* **2012**, *124*, 2060; *Angew. Chem. Int. Ed.* **2012**, *51*, 2020; c) H. Usta, A. Facchetti, T. J. Marks, *Acc. Chem. Res.* **2011**, *44*, 501; d) F. S. Kim, G. Ren, S. A. Jenekhe, *Chem. Mater.* **2011**, *23*, 682; e) A. R. Murphy, J. M. J. Fréchet, *Chem. Rev.* **2007**, *107*, 1066; f) S. Allard, M. Forster, B. Souharce, H. Thiem, U. Scherf, *Angew. Chem.* **2008**, *120*, 4138; *Angew. Chem. Int. Ed.* **2008**, *47*, 4070; g) F. Würthner, *Angew. Chem.* **2001**, *113*, 1069; *Angew. Chem. Int. Ed.* **2001**, *40*, 1037; h) A. Facchetti, *Chem. Mater.* **2010**, *23*, 733.

[2] a) J. E. Anthony, A. Facchetti, M. Heeney, S. R. Marder, X. Zhan, *Adv. Mater.* **2010**, *22*, 3876; b) Y. Wen, Y. Liu, *Adv. Mater.* **2010**, *22*, 1331; c) J. Zaumseil, H. Sirringhaus, *Chem. Rev.* **2007**, *107*, 1296; d) C. R. Newman, C. D. Frisbie, D. A. da Silva Filho, J.-L. Brédas, P. C. Ewbank, K. R. Mann, *Chem. Mater.* **2004**, *16*, 4436; e) C. J. Tonzola, M. M. Alam, W. Kaminsky, S. A. Jenekhe, *J. Am. Chem. Soc.* **2003**, *125*, 13548; f) A. Babel, S. A. Jenekhe, *J. Am. Chem. Soc.* **2003**, *125*, 13656.

[3] a) F. Babudri, G. M. Farinola, F. Naso, R. Ragni, *Chem. Commun.* **2007**, 1003; b) M.-H. Yoon, S. A. DiBenedetto, A. Facchetti, T. J. Marks, *J. Am. Chem. Soc.* **2005**, *127*, 1348; c) A.

Facchetti, M. Mushrush, M.-H. Yoon, G. R. Hutchison, M. A. Ratner, T. J. Marks, *J. Am. Chem. Soc.* **2004**, *126*, 13859.

[4] a) X. Guo, F. S. Kim, M. J. Seger, S. A. Jenekhe, M. D. Watson, *Chem. Mater.* **2012**, *24*, 1434; b) J. L. Segura, H. Herrera, P. Bäuerle, *J. Mater. Chem.* **2012**, *22*, 8717; c) F. Würthner, M. Stolte, *Chem. Commun.* **2011**, *47*, 5109; d) E. Ahmed, G. Ren, F. S. Kim, E. C. Hollenbeck, S. A. Jenekhe, *Chem. Mater.* **2011**, *23*, 4563; e) L. E. Polander, S. P. Tiwari, L. Pandey, B. M. Seifried, Q. Zhang, S. Barlow, C. Risko, J.-L. Brédas, B. Kippelen, S. R. Marder, *Chem. Mater.* **2011**, *23*, 3408; f) X. Zhan, A. Facchetti, S. Barlow, T. J. Marks, M. A. Ratner, M. R. Wasielewski, S. R. Marder, *Adv. Mater.* **2011**, *23*, 268; g) F. S. Kim, X. Guo, M. D. Watson, S. A. Jenekhe, *Adv. Mater.* **2010**, *22*, 478; h) H. Yan, Z. Chen, Y. Zheng, C. Newman, J. R. Quinn, F. Dotz, M. Kastler, A. Facchetti, *Nature* **2009**, *457*, 679; i) A. L. Briseno, S. C. B. Mannsfeld, C. Reese, J. M. Hancock, Y. Xiong, S. A. Jenekhe, Z. Bao, Y. Xia, *Nano Lett.* **2007**, *7*, 2847; j) H. E. Katz, A. J. Lovinger, J. Johnson, C. Kloc, T. Siegrist, W. Li, Y. Y. Lin, A. Dodabalapur, *Nature* **2000**, *404*, 478.

[5] a) R. P. Ortiz, H. Herrera, C. Seoane, J. L. Segura, A. Facchetti, T. J. Marks, *Chem. Eur. J.* **2012**, *18*, 532; b) M. Gsänger, J. H. Oh, M. Könemann, H. W. Höffken, A.-M. Krause, Z. Bao, F. Würthner, *Angew. Chem.* **2010**, *122*, 752; *Angew. Chem. Int. Ed.* **2010**, *49*, 740; c) R. Schmidt, J. H. Oh, Y.-S. Sun, M. Deppisch, A.-M. Krause, K. Radacki, H. Braunschweig, M. Könemann, P. Erk, Z. Bao, F. Würthner, *J. Am. Chem. Soc.* **2009**, *131*, 6215.

[6] a) S.-L. Suraru, U. Zschieschang, H. Klauk, F. Würthner, *Chem. Commun.* **2011**, *47*, 11504; b) Y. Zhao, C.-A. Di, X. Gao, Y. Hu, Y. Guo, L. Zhang, Y. Liu, J. Wang, W. Hu, D. Zhu, *Adv. Mater.* **2011**, *23*, 2448; c) Y. Avlasevich, C. Li, K. Müllen, *J. Mater. Chem.* **2010**, *20*, 3814.

[7] D. Izuhara, T. M. Swager, *J. Am. Chem. Soc.* **2009**, *131*, 17724.

[8] Y. Zhu, C.-T. Yen, S. A. Jenekhe, W.-C. Chen, *Macromol. Rapid Commun.* **2004**, *25*, 1829.

[9] CCDC 915892 contains the supplementary crystallographic data for this paper. These data can be obtained free of charge from The Cambridge Crystallographic Data Centre via www.ccdc.cam.ac.uk/data_request/cif.

[10] A. Hérold in *Physics of Intercalation Compounds* (Eds.: L. Pietronero, E. Tosatti), Springer, Berlin, **1981**, p. 7.

[11] a) S. A. Jenekhe, L. D. Lu, M. M. Alam, *Macromolecules* **2001**, *34*, 7315; b) Y. Zhu, R. D. Champion, S. A. Jenekhe, *Macromolecules* **2006**, *39*, 8712.

[12] S. Subramaniyan, H. Xin, F. S. Kim, S. Shoaee, J. R. Durrant, S. A. Jenekhe, *Adv. Energy Mater.* **2011**, *1*, 854.

